



HAL
open science

Multinuclear NMR as a tool for studying local order and dynamics in $\text{CH}_3\text{NH}_3\text{PbX}_3$ ($\text{X} = \text{Cl}, \text{Br}, \text{I}$) hybrid perovskites

Claire Roiland, Gaelle Trippé-Allard, Kaoula Jemli, Bruno Alonso, Jean-Claude Ameline, Regis Gautier, Thierry Bataille, Laurent Le Polles, Emmanuelle Deleporte, Jacky Even, et al.

► To cite this version:

Claire Roiland, Gaelle Trippé-Allard, Kaoula Jemli, Bruno Alonso, Jean-Claude Ameline, et al.. Multinuclear NMR as a tool for studying local order and dynamics in $\text{CH}_3\text{NH}_3\text{PbX}_3$ ($\text{X} = \text{Cl}, \text{Br}, \text{I}$) hybrid perovskites. *Physical Chemistry Chemical Physics*, 2016, Physical chemistry of hybrid perovskite solar cells, 18 (39), pp.27133-27142. 10.1039/C6CP02947G . hal-01354947

HAL Id: hal-01354947

<https://hal.science/hal-01354947>

Submitted on 24 Nov 2016

HAL is a multi-disciplinary open access archive for the deposit and dissemination of scientific research documents, whether they are published or not. The documents may come from teaching and research institutions in France or abroad, or from public or private research centers.

L'archive ouverte pluridisciplinaire **HAL**, est destinée au dépôt et à la diffusion de documents scientifiques de niveau recherche, publiés ou non, émanant des établissements d'enseignement et de recherche français ou étrangers, des laboratoires publics ou privés.

Copyright

Multinuclear NMR as a tool for studying local order and dynamics in $\text{CH}_3\text{NH}_3\text{PbX}_3$ ($\text{X} = \text{Cl}, \text{Br}, \text{I}$) hybrid perovskites

Claire Roiland,^a Gaëlle Trippé-Allard,^b Khaoula Jemli,^b Bruno Alonso,^c Jean-Claude Ameline,^d Régis Gautier,^a Thierry Bataille,^a Laurent Le Pollès,^{a,t} Emmanuelle Deleporte,^b Jacky Even,^{e,t} and Claudine Katan^{a,t}

We report on ^{207}Pb , ^{79}Br , ^{14}N , ^1H , ^{13}C and ^2H NMR experiments for studying the local order and dynamics in hybrid perovskite lattices. ^{207}Pb NMR experiments at room temperature on a series of MAPbX_3 compounds ($\text{MA} = \text{CH}_3\text{NH}_3^+$; $\text{X} = \text{Cl}, \text{Br}$ and I) showed that the isotropic ^{207}Pb NMR shift is strongly dependent on the nature of the halogen ions. Therefore ^{207}Pb NMR appears to be a very promising tool for the characterisation of local order in mixed halogen hybrid perovskites. ^{207}Pb NMR on MAPbBr_2I served as a proof of concept. Proton, ^{13}C and ^{14}N NMR experiments confirmed the results previously reported in the literature. Low temperature deuterium NMR measurements, down to 25K, were carried out to investigate the structural phase transitions of MAPbBr_3 . Spectral lineshapes allow following the successive phase transitions of MAPbBr_3 . Finally, quadrupolar NMR lineshapes recorded in the orthorhombic phase were compared with simulated spectra, using DFT calculated electric field gradients (EFG). Computed data do not take into account any temperature effect. Thus, the discrepancy between the calculated and experimental EFG evidences the fact that MA cations are still subject to significant dynamics, even at 25K.

Introduction

Halide perovskite solar cells proposed recently¹⁻⁹ have reached in a few years record photoconversion efficiencies matching in 2016 (22.1%) the best existing thin film technologies, namely CdTe (22.1%) and CIGS (22.3%).¹⁰ Perovskite cell photoconversion efficiencies are coming closer to the one of silicon (25%),¹⁰ but numerous issues (up scaling, resistance to moisture and light soaking, hysteresis ...) have to be overcome before reaching a possible industrialization. Chemical engineering afforded by the hybrid perovskite materials may provide a variety of applications such as tandem solar cells, light emitters or detectors. Ongoing perovskite cell developments toward higher solar cell efficiencies are based on complex alloys involving both mixings of cations such as methyl ammonium (MA^+), formamidinium (FA^+) and Cs^+ , and halide anions.⁷⁻⁹ Most important experimental results were obtained in the initial period of perovskite solar cell research (2007-2014) for MAPbX_3 where $\text{X} = \text{I}, \text{Br}, \text{Cl}$.¹⁻⁶ Prior to that, MAPbX_3 bulk materials were the subject of quite a few fundamental studies, including nuclear magnetic resonance (NMR) spectroscopy,^{11,12} dielectric and millimetre wave measurements,^{13,14} calorimetry,¹⁵ optical characterizations techniques^{16,17} as well as X-ray diffraction.^{18,19}

The isostructural MAPbX_3 hybrid perovskites have a primitive cubic structure at high temperature and undergo a cubic (Pm-3m) to tetragonal (I4/mcm) antiferrodistorsive phase transition at $T_c \sim 327\text{K}$, 237K and 179K for $\text{X} = \text{I}, \text{Br}$ and Cl ,¹³ respectively. Given the symmetry of the organic cation, MA are necessarily disordered in both the cubic (α -phase) and tetragonal (β -phase) phases. At lower temperatures (162K, 149-154K and 173K, respectively)¹³ the tetragonal phase transforms to an orthorhombic (Pnma ; γ -phase) system.

Solar cells using MAPbBr_3 have been demonstrated, but the bulk material has not an optimum electronic band gap for a single junction cell compared to the ones based on MAPbI_3 .²⁰⁻²² Nevertheless, MAPbBr_3 may lead to a number of possible

applications based on electronic band gap tuning for tandem cell applications or in the composition of alloys which stabilizes the halide perovskite structure.²³⁻²⁸ Moreover, MAPbBr_3 bulk material has other interesting intrinsic optoelectronic properties,²⁹⁻³³ which are enhanced in colloidal nanostructures.³⁴⁻³⁶ A number of operating light emitting devices based on MAPbBr_3 have indeed been demonstrated.^{29,37-41} Recent progresses in halide perovskite synthesis and crystal growth allowed going deeper into the understanding of the bulk properties of MAPbX_3 materials, especially for the bromide compound.⁴²⁻⁵¹ For instance, recent diffraction and NMR investigations gave better insight into the structural and the dynamical properties of MAPbBr_3 .⁵⁰⁻⁵¹

A complex dynamical picture has progressively emerged for MAPbX_3 bulk materials, which combine highly anharmonic lattice vibrations and stochastic MA reorientations, at high temperature. These properties significantly influence the optoelectronic and thermal properties.⁵²⁻⁶⁰ The freezing of the MA cation dynamics at low temperature has recently been interpreted as a transition from a plastic crystal phase to an orientational glass.⁶⁰ Although this theoretical prediction agrees with recent experimental data,⁶¹ further experimental investigations are required.

Compared to the numerous diffraction studies devoted to MAPbX_3 , local structural information using resonance techniques is still scarce.^{11,12,51} Meanwhile, solid-state NMR is a tool able to probe dynamics in the solid state in several ranges of frequency. Diverse NMR approaches are available to probe such a dynamics. For instance, T_1 relaxation measurements allow probing the dynamics in the Larmor frequency range (typically 10 MHz to 1 GHz). In a very different frequency range, NMR exchange experiments allow to evidence motion from the Hz to the kHz. Dynamics can also induce lineshape modifications by partially or fully averaging first order anisotropies (chemical shift or first order quadrupolar interaction) or second order quadrupolar anisotropies. In that case, NMR experiments are sensitive to motion at frequencies

between a kHz and a few hundreds of kHz. The dynamic lineshape modifications are sensitive both to the frequency and the geometry of the motion.

Most of the nuclei present in hybrid perovskites can be probed; however they exhibit different spectroscopic properties. ^1H is a spin- $\frac{1}{2}$ nucleus presenting strong dipolar interactions in a solid without dynamics. Deuterium ($I=1$, Natural Abundance (N.A.) = 0.015%) can be employed on deuterium-enriched samples. It usually leads to spectra dominated by first order quadrupolar interactions. ^{13}C ($I=1/2$) has a low natural abundance (NA = 1.1%). In the solid state, ^{13}C nuclei usually present strong dipolar interactions with the surrounding protons. In a solid without fast dynamics, this allows to record ^{13}C spectra by using CPMAS (Cross Polarization Magic Angle Spinning) type experiments. Direct ^{13}C acquisition can be an option in the case of a solid presenting fast dynamics. Nitrogen can also be addressed either by ^{15}N ($I = 1/2$, N.A. = 0.37%) or ^{14}N ($I = 1$, N.A. = 99.63%) NMR. The isotropic chemical shift of ^{207}Pb ($I=1/2$, N.A. = 22.1 %) covers a broad range, of more than 5000 ppm, and presents usually large chemical shift anisotropies. On the halogen side, all the halogen nuclei can potentially be probed by NMR.^{62,63} However, both chlorine and iodine are very challenging nuclei for NMR spectroscopy due to their low gyromagnetic ratios and/or high quadrupolar moments. ^{79}Br ($I=3/2$, N.A. = 50.54 %) has a relatively large quadrupolar moment but seems to be the best halogen nucleus to probe hybrid perovskite materials. Among these probes, Wasylshen and co-workers have already investigated ^2H and ^{14}N ,^{11,12} whereas Baikie and co-workers focused on ^1H and ^{13}C .⁵¹

In the present work, we report on NMR recorded on MAPbX_3 ($X = \text{I, Br, Cl}$) powders. This includes ^{207}Pb , ^{79}Br , ^{14}N , ^1H , ^{13}C and ^2H NMR experiments. Room temperature ^1H , ^{13}C and ^{14}N are performed using Magic Angle Spinning (MAS) NMR. ^{14}N was probed between 233 and 333K. Static deuterium NMR investigations were carried out at various temperatures, down to 25K. Results are in fair agreement with available data from the literature. Moreover, we show that both ^{207}Pb and ^{79}Br NMR are of particular relevance to study local environments in hybrid perovskites. Last, temperature dependant follow-up of deuterium NMR on MAPbBr_3 is shown to provide further insight on the dynamics of the molecular moieties, *i.e.* the MA cations.

Experimental

Synthetic procedures

General procedure for synthesis of methylammonium- d_3 tribromide (deuterium enrichment). Hydrobromic acid (47% - 4 mL) and deuterium oxide (4 mL) are stirred during one hour. The solution is cooled to 2°C before adding methylamine 2.0M in methanol (5mL, 2 mmol). The mixture is stirred during 2 hours at 2°C, before being concentrated in vacuum. The powder is rinsed with diethyl ether and dried in oven at 50°C during 3 hours.

General procedure for synthesis of methylammonium- d_3 lead tribromide. To a colourless solution of lead bromide (367 mg, 1

mmol) in DMF (10 mL), methyl bromide (white powder - 115 mg, 1 mmol) is added. The solution remains colourless. The agitation is extended during 15 mn before evaporation of solvent. The resulting orange powder is successively washed with acetone and diethyl ether. The orange powder is dried at 60°C during 1hour. Yield: 97% (469 mg).

General procedure for synthesis of methylammonium lead triiodide / $\text{CH}_3\text{NH}_3\text{PbI}_3$. To a colourless solution of lead iodide (922 mg, 2 mmol) in GBL (10 mL), methyl iodide (white powder - 318 mg, 2 mmol) is added. The yellow solution is stirred during 5 mn before evaporation of solvent. The resulting black powder is successively washed with acetone and diethyl ether. The orange powder is dried at 60°C during 1hour. Yield: 85% (1.05 g).

General procedure for synthesis of methylammonium lead tribromide / $\text{CH}_3\text{NH}_3\text{PbBr}_3$. To a colourless solution of lead bromide (734 mg, 2 mmol) in DMF (20 mL), methyl bromide (white powder - 224 mg, 2 mmol) is added. The solution remains colourless. The agitation is extended during 5 mn before evaporation of solvent. The resulting orange powder is successively washed with acetone and diethyl ether. The orange powder is dried at 60°C during 1hour. Yield: 82% (790 mg).

General procedure for synthesis of methylammonium lead trichloride / $\text{CH}_3\text{NH}_3\text{PbCl}_3$. To a colourless solution of lead chloride (973 mg, 3.5 mmol) in DMSO (30 mL), methyl chloride (white powder - 263.5 mg, 3.5 mmol) is added. The solution remains colourless. The agitation is extended during 5 mn after completed solubilisation, and then the solvent is removed. The resulting white powder is successively washed with acetone and diethyl ether. The white powder is dried at 60°C during 1hour. Yield: 84% (1.04 g).

General procedure for synthesis of methylammonium lead dibromide iodide / $\text{CH}_3\text{NH}_3\text{PbIBr}_2$. To a colourless solution of lead bromide (367 mg, 1 mmol) in DMF (10 mL), methyl iodide (white powder - 159 mg, 1 mmol) is added. The solution becomes yellow instantaneously. The agitation is extended during 5 mn before evaporation of the solvent. The resulting maroon powder is successively washed with acetone and diethyl ether. The maroon powder is dried at 60°C during 1hour. Yield: 53% (280 mg).

NMR spectroscopy

Room temperature solid-state NMR for ^1H , ^{13}C , ^{207}Pb , ^{79}Br . Magic Angle Spinning (MAS) solid-state NMR experiments were performed on a Bruker Avance III 600 SB spectrometer (magnetic field : 14T) operating at Larmor frequencies of 600.1 MHz for ^1H , 150.9 MHz for ^{13}C , 125.5 MHz for ^{207}Pb and 150.3 MHz for ^{79}Br . Solid-state NMR spectra were recorded using a 3.2 mm MAS (Magic Angle Spinning) double resonance probehead, and MAS frequencies were set to 5 kHz for ^1H and ^{13}C and 22 kHz for ^{207}Pb and ^{79}Br . Longitudinal and transverse relaxation times, T_1 and T_2^* , were measured using a saturation/recovery sequence and a 2D spin-echo, respectively. Those measurements made us certain that using a recycle delay set to 1s is long enough to ensure a full relaxation of the spins system. ^1H and ^{207}Pb were acquired using a 90° single pulse corresponding to a radio frequencies of 114 kHz and 58 kHz, respectively. To avoid

lineshape distortion due to the quadrupolar effect, ^{79}Br spectrum was acquired using a single pulse corresponding to a flip angle of 6° . Cross polarisation (CP) ^{13}C spectra were performed using a ^1H to ^{13}C transfer delay set to 2 ms. A proton decoupling pulse (46 kHz) was applied during the acquisition. Static ^{207}Pb NMR experiments were performed on a Bruker Avance I 300 WB spectrometer (7T) operating at Larmor frequency (62.7 MHz) using a 4 mm MAS double resonance probehead. In order to avoid baseline distortion, static NMR spectra were measured using a spin echo sequence. The echo delay is set to $6.7\ \mu\text{s}$, 90° pulse to $2.2\ \mu\text{s}$ and recycle delay to 1 s. Whenever possible, static experiments were preferred instead of MAS, to avoid possible degradation of the sample caused by the light beam used to detect the rotational speed of the rotor and/or the sample heating due to frictions occurring in fast spinning MAS rotors. In addition, ^1H spectra were conducted regularly to check the quality of the samples. ^1H and ^{13}C chemical shifts were referenced to TMS. ^{207}Pb and ^{79}Br chemical shifts were referenced to $\text{Pb}(\text{NO}_3)_2$ and a solution 0.01M of NaBr in D_2O , respectively. Fits were performed using the dmfit software⁷⁶.

Room temperature solid-state NMR for ^{14}N . ^{14}N NMR spectra were performed on a 600 Varian spectrometer (14T) operating at Larmor frequency of 43.3 MHz using a 9.5 mm rotors. Single pulse MAS spectra were acquired using a 30° flip angle, a recycle delay set at 1 s and a MAS frequency set at 3.5 kHz. Temperature experiments were done from 233K to room temperature. For each temperature, the longitudinal relaxation time T_1 was measured using a saturation/recovery sequence. ^{14}N chemical shifts were referenced to NH_4Cl .

Variable temperature solid-state NMR: ^2H . ^2H low temperature NMR experiments were performed on a Bruker Avance I 300 WB spectrometer (magnetic field: 7T) operating at Larmor frequencies of 46 MHz for ^2H . To allow low temperature measurements, the shims were removed and replaced by an Oxford cryostat. Deuterated hybrid perovskite was packed in a 6 mm Teflon tube and placed in a homemade very low temperature probe (up to 4K). ^2H spectra were recorded under static condition using a solid echo sequence and VOCS.⁷⁹ The 90° pulse corresponds to a RF field of 27.5 kHz and the echo delay was set to $150\ \mu\text{s}$. Temperature was set using an Oxford temperature regulating system using liquid nitrogen as cryogenic fluid.

Computational details. Calculations on $\text{CH}_3\text{NH}_3\text{PbBr}_3$ were carried out using the CASTEP 6.0 DFT code that explicitly describes the crystalline structure of the compounds using periodic boundary conditions.^{80,81} The orthorhombic crystal structure of $\text{CH}_3\text{NH}_3\text{PbBr}_3$ determined by Swinson and coworkers was considered.¹⁸ Only Hydrogen atoms were free to relax. The exchange-correlation interaction was described within the generalized gradient approximation (GGA) of Perdew, Burke, and Ernzerhof.⁸² All ultrasoft pseudopotentials (US-PP) were generated using the OTF_ultrasoft pseudo-potential generator included in CASTEP 6.0. The PAW formalism was used to calculate the EFG tensors from the pseudodensity.^{83,84} The EFG tensor is traceless; *i.e.* its eigenvalues (V_{xx} , V_{yy} , and V_{zz}) obey $V_{xx} + V_{yy} + V_{zz} = 0$. We used the following conventions for the quadrupolar coupling constant C_Q and the asymmetry parameter η_Q : $C_Q = eQV_{zz}/h$ and $\eta_Q = (V_{xx} - V_{yy})/V_{zz}$ with $|V_{zz}| \geq |V_{xx}| \geq |V_{yy}|$. A quadrupolar moment Q for ^2H equal to 2.86

$10^{-29}\ \text{m}^2$ was used. All calculations were proven to converge in NMR values with a cutoff energy of 800 eV. The Monkhorst–Pack k-point grid density used was densified until convergence.⁸⁵ Relativistic effects were included for all elements during the US-PP generation by solving the scalar relativistic equation of Koelling and Harmon.⁸⁶ Non-linear core corrections have been applied to all atoms.⁸⁷

X-ray powder diffraction. The pattern of $\text{CH}_3\text{NH}_3\text{PbBr}_2\text{I}$ was collected at room temperature using a PANalytical Empyrean diffractometer, with the $\text{Cu}\ K\alpha$ radiation ($K\alpha_1 = 1.5406\ \text{\AA}$, $K\alpha_2 = 1.5444\ \text{\AA}$) selected with the Bragg-Brentano HD device (flat multilayer X-ray mirror) from PANalytical.

Results and discussion

^{79}Br NMR

Chlorine, bromine and iodine are all quadrupolar nuclei ($I > 1/2$). Among all the three halogen nuclei probed, significant NMR signal was only obtained for ^{79}Br in MAPbBr_3 . We were not able to record any ^{127}I NMR spectra from MAPbI_3 . The latter is in the tetragonal phase at room temperature and presumably presents a large quadrupolar interaction, preventing its acquisition by standard NMR techniques.

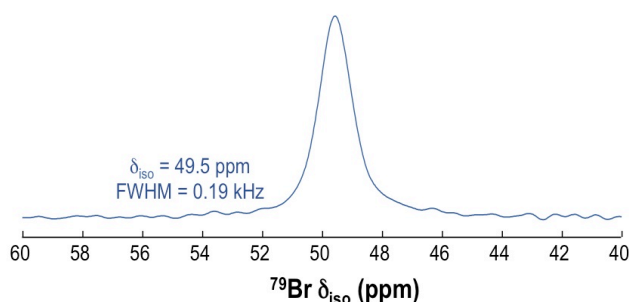


Figure 1. ^{79}Br MAS NMR spectrum obtained at 14T on MAPbBr_3 .

The ^{79}Br spectrum is sketched in Figure 1. It presents a single narrow resonance located at 49.5 ppm. This spectrum does not exhibit any feature of a quadrupolar interaction confirming the high symmetry of the bromine site and the cubic structure of MAPbBr_3 at room temperature. In the case of compounds with lower symmetry crystal structures, the high quadrupolar moment of ^{79}Br often gives rise to highly complex NMR lineshapes. In the present work, we did not investigate further ^{79}Br NMR in MAPbBr_3 . However, we suggest the use of high field ^{79}Br NMR (18T or more) experiments to reduce the second order quadrupolar linewidth. In addition, $^{79/81}\text{Br}$ NQR experiments⁶⁴ may be relevant to investigate distributions of bromine in mixed halide perovskites.⁶⁵

^{207}Pb NMR

^{207}Pb is a spin- $1/2$ nucleus presenting a large range of chemical shift (at least 5000 ppm) and usually large chemical shift anisotropies. It has already been employed for the characterisation of inorganic materials,^{63,66-68} but not in lead-based hybrid perovskites to the best of our knowledge.

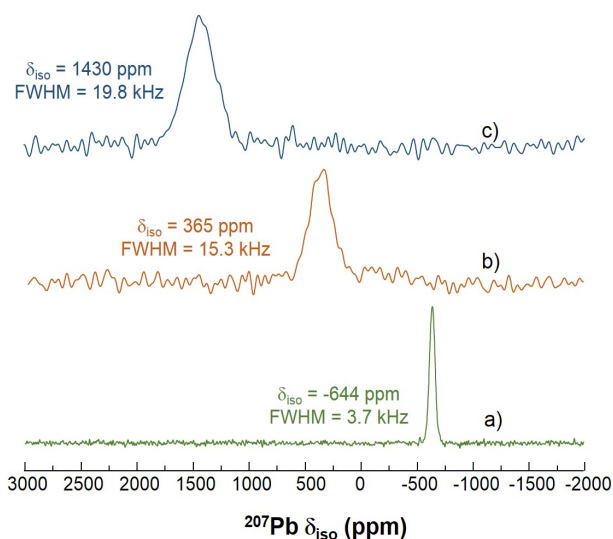


Figure 2. ^{207}Pb NMR spectra obtained at 7 T for MAPbCl_3 (a), MAPbBr_3 (b) and MAPbI_3 (c).

There are major interests in using ^{207}Pb NMR as a probe in the present context of hybrid perovskites. Even though the materials used for practical applications contain various chemical substitutions on the organic and halogen parts of the structure, lead is still massively used as a metal centre. Therefore ^{207}Pb NMR spectroscopy would be central to evaluate locally the structural effect of the various substitutions. Furthermore, the lead ions are playing a key role in the density of states at the Fermi level since VB is dominantly controlled by a combination of lead s -orbitals and halide p -orbitals, and the CB relies mainly on the lead p -orbitals. Consequently the evolution of lead NMR chemical shift is directly related to the band structure at the Fermi level.

Static ^{207}Pb spectra are sketched in Figure 2. ^{207}Pb NMR appears to be highly sensitive to the chemical composition of MAPbX_3 compounds. Noteworthy, the ^{207}Pb spectrum of PbI_2 has recently been reported.⁶³ From the spectrum shown in Figure 2, we can conclude on the absence of any PbI_2 impurity in our MAPbI_3 powders. Static and MAS (Figure S1) spectra exhibit single lines consistent with a single lead site in the perovskite structure.

One can observe a general trend in the isotropic chemical shifts and in the spectra linewidth: going from chlorine to bromine and iodine, the isotropic shifts are -644 ppm, 365 ppm and 1430 ppm, respectively; the corresponding linewidths (FWHM) amount to 3.7, 15.3 and 19.8 kHz, respectively. Thus, the isotropic shift values and the linewidth of the Pb^{2+} ions are increasing while the halogen in its vicinity is getting heavier.

A similar trend is observed for the relaxation times T_1 (Table 1). On the contrary, the T_2 transverse relaxation times are quite comparable for MAPbCl_3 and MAPbBr_3 , while their linewidths are completely different (3.7 kHz and 15.3 kHz, respectively). These T_2 values confirm that the linewidth is not only due to a relaxation effect.

Table 1 ^{207}Pb Longitudinal and transverse relaxation times, noted as T_1 and T_2^* , respectively, measured for MAPbX_3 compounds. T_1 values are obtained using a saturation/recovery sequence under MAS. T_2^* are measured according to a 2D spin-echo under MAS. T_2^* for MAPbI_3 is too short to produce measurable results under rotor synchronised conditions.

	T_1 (ms)	T_2^* (ms)
MAPbCl_3	900	75
MAPbBr_3	185	70
MAPbI_3	50	--

Further investigations at different magnetic fields (\vec{B}) and temperatures (T) are needed to rationalize these findings. For instance, such experiments may provide indications of whether or not a distribution of chemical shifts (\vec{B}) or changes of the chemical shift tensor related to the dynamics (T) are at work. Moreover, these results suggest that ^{207}Pb NMR spectroscopy should provide an appropriate tool to investigate mixed compositions.

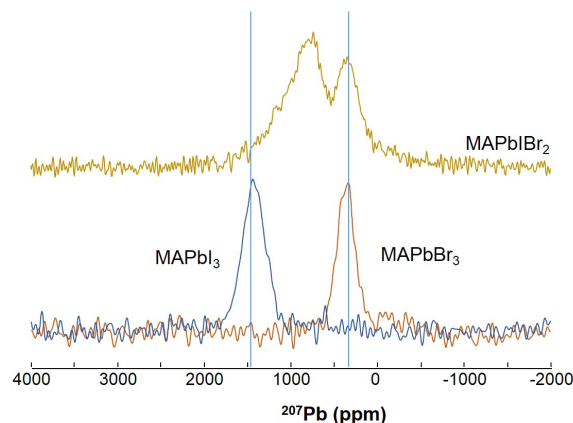


Figure 3. ^{207}Pb NMR spectra obtained at 7 T for MAPbCl_3 (a), MAPbBr_3 (b) and MAPbI_3 (c).

In order to provide a proof of concept, we further investigate a mixed halide solid solution, namely a powder of MAPbBr_2I . The ^{207}Pb NMR spectrum shown Figure 3 exhibits an NMR signal with two components, the first one at 795 ppm and a second one at 347 ppm. The latter corresponds to the position of the signal obtained for the MAPbBr_3 powder. This raises the question of whether the I/Br distribution is homogeneous. To find out whether the MAPbBr_2I powder undergoes phase separation, we subsequently performed an X-Ray diffraction (XRD) analysis. Indexing the XRD powder diffraction pattern (Figure S2) clearly evidences that MAPbBr_2I is a phase pure product, with a cubic unit cell parameter of 6.0095(7) Å. Thus, it belongs to a solid solution, with no indication of the presence of the MAPbI_3 and MAPbBr_3 poles.

Two facts must be kept in mind for the interpretation of the ^{207}Pb NMR spectrum of MAPbBr_3 . Firstly, we may stress here that the spectrometer used to record the ^{207}Pb spectrum of the MAPbBr_2I powder has a filament lamp left on continuously. Thus, possible phase separation (MAPbI_3 and

MAPbBr₃) during the NMR acquisition followed by a return to a solid solution MAPbIBr₂ single phase cannot fully be ruled out. Secondly, the significantly lower T₂ relaxation time of MAPbI₃ as compared to MAPbBr₃ (Table 1) hampers any quantitative analysis of the ²⁰⁷Pb spectrum. As a matter of fact, the Hahn echo experiment will overestimate the intensities of the species presenting the largest T₂ relaxation.

Despite these limitations that may be circumvented by using alternative equipment, this result shows the complementarity for the structural studies performed by XRD and solid state NMR. The diffraction measurement reveals a long-range order averaged out among the sample volume, leading to an average unit cell. On the contrary, the ²⁰⁷Pb NMR experiment gives a much more local description. The interpretation we can make of the two contributions observed in the ²⁰⁷Pb NMR spectrum of MAPbBr₂I is that it allows to distinguish between the lead atoms connected to six bromine ions and those connected to both iodine and bromine. Clearly, the detailed understanding of the local structure of solid solutions, including their possible degradation under irradiation, requires complementary experimental and theoretical investigations, which are beyond the scope of the present work. However, we established that ²⁰⁷Pb NMR is an important tool to study the stability and the local ordering of mixed halide hybrid perovskites.

Light nuclei NMR results

¹H NMR experiments were carried out at 14 T under MAS conditions. Spectra are shown in Figure 4. For the three MAPbX₃ compounds, spectra exhibit two signals corresponding to NH₃ (about 6.5 ppm) and CH₃ (about 3.5 ppm) protons. These results are consistent with those carried out at 9.4 T by Baikie and coworkers.⁵¹ Moreover, the increase of the apparent linewidth is connected to the increase of the halogen mass. Several spinning sidebands (SSb) are observed for each member of the MAPbX₃ series. Since the proton residual dipolar coupling cannot be neglected in this case, the SSb pattern cannot be fitted in order to extract the chemical shift tensor, as it is commonly done for slow MAS spectra.⁶⁹ Nevertheless, the SSb pattern is identical for the three MAPbX₃ compounds and does not appear discriminant for structural phase identification.

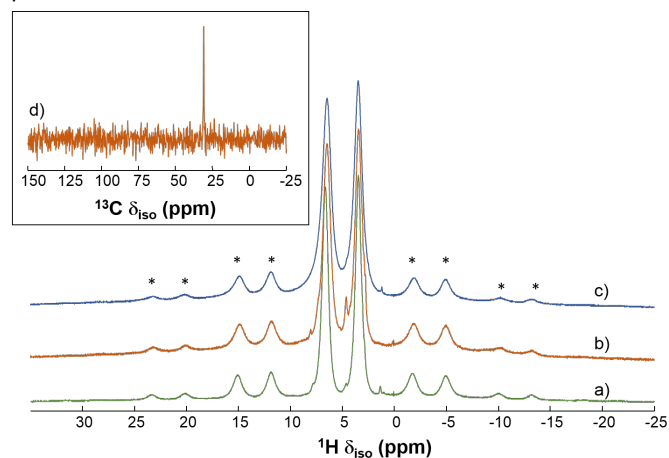


Figure 4. ¹H MAS NMR spectra obtained at 14 T under MAS condition for MAPbCl₃ (a), MAPbBr₃ (b) and MAPbI₃ (c). Spinning sidebands are marked with asterisks. Insert: ¹³C CPMAS spectra obtained on MAPbBr₃.

¹³C CPMAS NMR analysis (insert in Figure 4) is consistent with the presence of methyl groups. The isotropic chemical shift is almost identical (about 31 ppm) for all the MAPbX₃ series. The weak signal observed by CPMAS was recorded using a relatively long CP experiment (14h). The difficulty to employ the CP experiment is probably due to a small residual dipolar coupling indicative of a fast dynamics of the MA cations at room temperature.

Despite its high natural abundance, ¹⁴N is a relatively challenging nucleus with an integer spin, a high quadrupolar coupling and a low gyromagnetic ratio (γ) that presents usually very broad NMR signal. Some recent developments open the way to improved acquisition and understanding of ¹⁴N NMR signals, particularly in the case of solid-state compounds that have interesting structural dynamics.⁷⁰⁻⁷¹

We performed ¹⁴N MAS NMR experiments on MAPbCl₃ at different temperatures, from 233K to 303K. The experimental spectra are sketched in Figure 5. In this temperature range, the spectrum presents a single isotropic resonance (arrow) located at 7 ppm and a SSb pattern with a Lorentzian shape and a 4 kHz linewidth. When decreasing the temperature, the isotropic resonance seems to become slightly broader (insert of Figure 5).

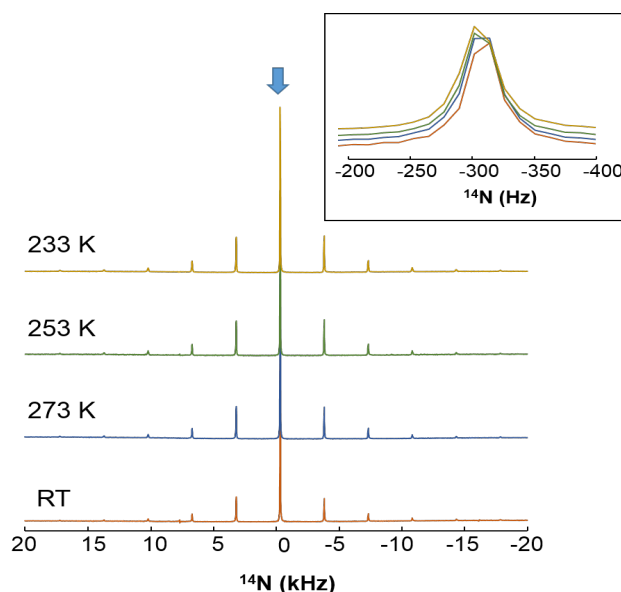


Figure 5. ¹⁴N MQS NMR spectra obtained on MAPbCl₃ from 233K to room temperature. Insert: focus on the isotropic resonance.

Table 2 : ¹⁴N T₁ values measured on MAPbCl₃ using a saturation/recovery pulse sequence according to the sample temperature

T (K)	T ₁ (ms)
333	280
293 (RT)	230
283	171
273	146
253	122
233	83

Concomitantly, the longitudinal relaxation time decreases significantly, from 280 ms to 83 ms (Table 2). This is a direct signature of the dynamics of the organic cation in the cubic phase. Assuming isotropic motion, namely an Arrhenius behaviour, would allow to extract the corresponding activation energy. However, consistently with earlier findings, we observed a non-Arrhenius behaviour which hinder the use of a simple BPP model for the data analysis.¹¹

Moreover, the isotropic lineshapes are consistent with an isotropic tumbling of the MA cations, at least down to 233 K. This is consistent with the lower transition temperature ($T < 179\text{K}$)^{13,15} of MAPbCl_3 , as compared to MAPbI_3 and MAPbBr_3 , for the structural phase transition from the cubic Pm-3m phase to an ordered low temperature phase.

Besides, these results obtained under magic angle spinning conditions are consistent with former static experiments by Wasylishen and co-workers.^{11,12} They suggest that ^{14}N NMR should provide an appropriate tool to further investigate the low temperature ordering expected in the MAPbX_3 phases.

Temperature-dependant ^2H NMR

Deuterium NMR lineshape modulations is a well-established tool to investigate the dynamics of molecules in the solid state⁷²⁻⁷⁵. To get insight in the dynamical behaviour of the MA cations, we use the dynamical modulation by the first order quadrupolar interaction on a partially deuterated MAPbBr_3 powder. These deuterium NMR experiments were carried out from room temperature down to 25K. Corresponding spectra are shown Figures 6-8.

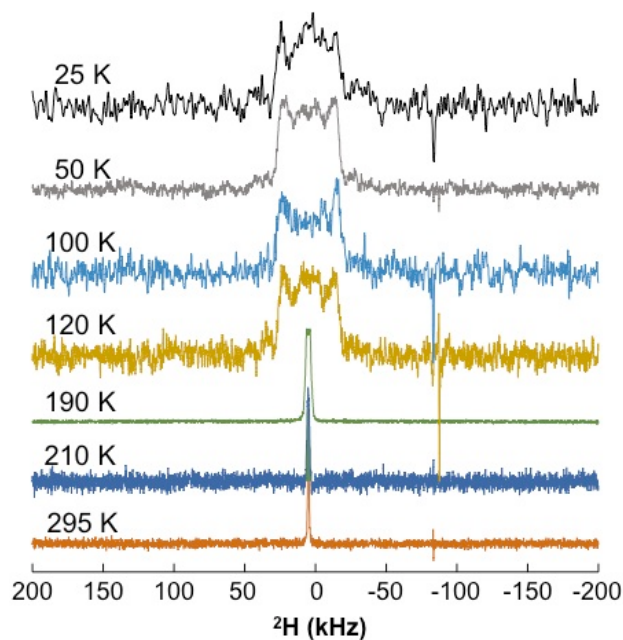


Figure 6. ^2H static NMR spectra recorded on $\text{CH}_3\text{ND}_3\text{PbBr}_3$ from room temperature to liquid He range temperature (down to 25 K).

In the cubic phase down to 233 K, the deuterium NMR lineshapes are fully isotropic, as already reported in the literature.^{11,12} These isotropic lineshapes recorded in the cubic phase are consistent with an overall orientation in a potential

with cubic symmetry. In other words, it is consistent with a dynamical stochastic tumbling of the C-N axis and concomitant fast rotational motion of the methyl and ammonium rotors.

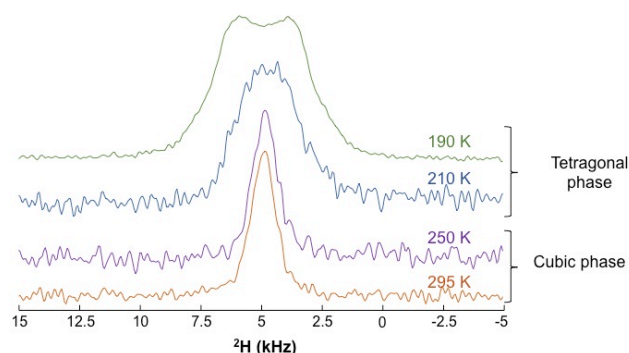


Figure 7. Zoom on the ^2H static NMR spectra shown of figure 5. Comparison of the lineshapes recorded in the cubic and tetragonal phases.

Figure 7 highlights the changes in spectral lineshape between the cubic and the tetragonal phase. A small first order quadrupolar splitting arises that increases as temperature diminishes. This temperature evolution of the quadrupolar splitting can be associated with a reduction of the isotropic motion of the principal axis of the methylammonium cation. Using the Dmfit software,⁷⁶ we extract the quadrupolar coupling constant (C_Q), which amounts to 4.1 kHz in the tetragonal phase at 190K, and a vanishing asymmetry parameter (η) (Figure 8).

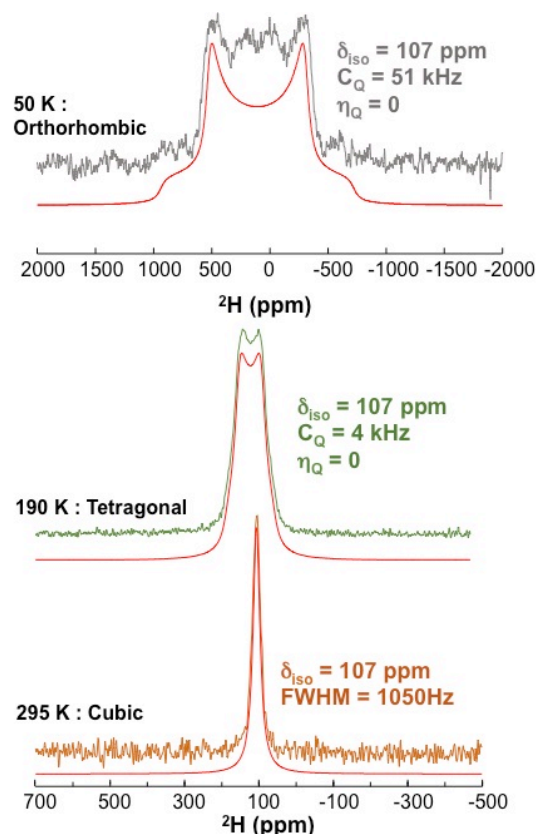


Figure 8. ^2H static NMR spectra (blue lines) and corresponding fitting results (red lines) in the three different crystallographic structures (cubic at RT, tetragonal at $T=190\text{K}$ and orthorhombic at $T=50\text{K}$) of MAPbBr_3 .

A further temperature decrease allows investigating the orthorhombic phase, between 148K and 25K, using a helium cryostat. At 25K, the deuterium T_1 seems to increase significantly making difficult the acquisition of spectra with good signal to noise ratio. The spectral lineshapes between 120K and 25K (Figure 6) clearly evidence much larger quadrupolar splitting than that observed in the tetragonal phase. However, this apparent quadrupolar splitting remains unchanged in the orthorhombic phase.

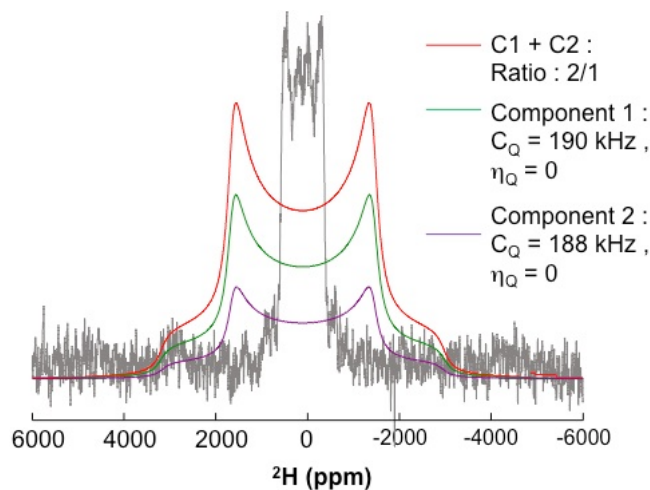


Figure 9. Comparison between the experimental ^2H lineshape obtained at 50 K (grey) on MAPbBr_3 and the simulated lineshapes according to the DFT computed EFG.

To get a better insight, we can refer to DFT calculations of the electric field gradient (EFG). They allow evaluating the static contribution of the crystal packing on the quadrupolar lineshape. According to available crystallographic data,¹⁸ two different deuterium sites are predicted in the orthorhombic $Pnma$ phase. However, the theoretical calculations yield very similar C_Q values for the two sites, 188 kHz (multiplicity 1) and 190 kHz, as well as very low η values (0.02). The spectral lineshapes deduced from the computed EFGs and measured experimentally are compared in Figure 9.

The obvious discrepancy between the computed static splitting and the experimental results, which is much larger than the one generally accepted between experimental and theoretical values,⁸⁸ reflects the partial motional narrowing of the EFG. It ranges from $\sim 188\text{-}190\text{kHz}$ to about 51kHz (Figure 9). This discrepancy reveals the dramatic effect of the methylammonium dynamics at low temperature. Meanwhile, the apparent quadrupolar splitting remains constant in the orthorhombic phase (Figure 6). These data suggest a fixed orientation of the CN axis. As the apparent splitting remains much smaller than the splitting calculated by DFT in the absence of dynamics, our results further suggest the presence of a fast rotational dynamics of the terminal methyl and ammonium groups.

For a more complete understanding of the dynamical behaviour of the MA cation across the different structural phase transitions, one may refer to complementary experimental and theoretical findings. Unfortunately, direct

experimental investigations of the MA cations in MAPbBr_3 by neutron scattering are scarce.⁵⁰ Detailed studies by inelastic incoherent neutron scattering are available for MAPbI_3 .^{77,78} Two quasi-elastic responses related to both MA tumbling dynamics and cation rotation around the C-N axis were described. The fast dynamics around the C-N axis at high temperature was reported to slow down at low temperature, but remaining active in the low temperature orthorhombic phase.⁷⁸ This observation is in line with the spectral narrowing observed in the present work, when compared to the static computations (Figure 9).

In addition, the complex deuterium NMR lineshapes (Figures 6-8) are compatible with previous theoretical predictions and recent experimental observations of an orientational glass behaviour in MAPbI_3 .^{60,61} Such an orientational glassy state at low temperature is expected to be related to a disordered freezing of the MA tumbling motions, *i.e.* the C-N axis. A static and random distribution of C-N axis orientations may strongly perturb the rotational motions around the C-N axis leading to a distribution of local dynamics. This issue deserves further study, for example, by performing solid-state NMR on deuterated single crystals.

Conclusions

This paper reports on extensive high-resolution solid-state NMR studies of MAPbX_3 powders, X = I, Br and Cl. Light nuclei NMR analysis based on ^1H , ^{13}C and ^{14}N are consistent with available data from the literature. The ^1H magic angle spinning spectra of all three MAPbX_3 compounds are almost identical. It is thus not discriminant for structural phase identification. Since the cross polarisation transfer is relatively inefficient and due to its low natural abundance, ^{13}C does not seem to be a relevant nucleus to probe hybrid perovskite structures. On the contrary, results obtained for ^{14}N NMR in the cubic phase are promising. Combined to the recent developments on ^{14}N NMR signal acquisition and understanding, this nucleus may represent an opportunity for further exploration of hybrid perovskites comprising at least one nitrogen atom, which is commonly found in the ammonium moiety of the organic cation.

We further show that among the halogen atoms, ^{79}Br may be the most relevant to study local distortions and distributions of halogens in mixed halide perovskites using high field NMR (18 T or more) or NQR spectroscopy.

Besides, we demonstrate that ^{207}Pb is highly sensitive to the nature of the halogen atom in MAPbX_3 compounds, with large differences in chemical shifts and linewidths. Our results strongly suggest that ^{207}Pb NMR spectroscopy is an excellent probe for lead-based hybrid perovskites and will be particularly useful in the context of the investigations of solid solutions, especially those based on a mix of halogen anions.

Finally, temperature-dependant deuterium NMR conducted on MAPbBr_3 samples proved to be efficient to investigate the structural phase transitions, the progressive freezing of the dynamics of principle axis of the MA cations and, from comparison to DFT computed EFG, the remaining fast rotational dynamics of the terminal methyl and ammonium

moieties. Although consistent with the existence of an orientational glassy behaviour at very low temperature,⁶⁰ more research is needed to confirm this trend, such as solid-state NMR or neutron, Raman and Brillouin scattering on both hydrogenated and deuterated single crystals.

Acknowledgements

This project has received funding from the European Union's Horizon 2020 research and innovation programme under the grant agreement No 687008. The information and views set out in this publication are those of the authors and do not necessarily reflect the official opinion of the European Union. Neither the European Union institutions and bodies nor any person acting on their behalf may be held responsible for the use which may be made of the information contained therein. Work at ISCR and FOTON was performed using grant from Cellule Energie du CNRS (SOLHYBTRANS Project) and the University of Rennes 1 (Action Incitative, Défis Scientifiques Emergents 2015). J. E. thanks the Fondation d'entreprises Banque Populaire de l'Ouest for its financial support (Grant PEROPHOT 2015). Rennes Métropole and Région Bretagne (FEDER) are acknowledged for funding the X-ray diffractometer.

Notes and references

- N. G. Park, *J. Phys. Chem. Lett.*, 2013, **4**, 2423.
- H. J. Snaith, *J. Phys. Chem. Lett.*, 2013, **4**, 3623.
- H. S. Kim, S. H. Im and N. G. Park, *J. Phys. Chem. C*, 2014, **118**, 5615.
- M. A. Green, A. Ho-Baillie and H. J. Snaith, *Nat. Photonics*, 2014, **8**, 506.
- P. Gao, M. Grätzel and M. K. Nazeeruddin, *Energy Environ. Sci.*, 2014, **7**, 2448.
- D. P. McMeekin, G. Sadoughi, W. Rehman, G. E. Eperon, M. Saliba, M. T. Horantner, A. Haghighirad, N. Sakai, L. Korte, B. Rech, M. B. Johnston, L. M. Herz and H. J. Snaith, *Science*, 2016, **351**, 151.
- W. Nie, H. Tsai, R. Asadpour, J.-C. Blancon, A. Neukirch, G. Gupta, J. J. Crochet, M. Chhowalla, S. Tretiak, M. A. Alam, H.-L. Wang and A. Mohite, *Science*, 2015, **347**, 522.
- R. E. Beal, D. J. Slotcavage, T. Leijtens, A. R. Bowering, R. A. Belisle, W. H. Nguyen, G. F. Burkhard, E. T. Hoke and M. D. McGehee, *J. Phys. Chem. Lett.*, 2016, **7**, 746.
- M. Saliba, T. Matsui, J.-Y. Seo, K. Domanski, J.-P. Correa-Baena, K.-N. Mohammad, S. M. Zakeeruddin, W. Tress, A. Abate, A. Hagfeldt and M. Grätzel, *Energy Environ. Sci.*, 2016, **9**, 1989-1997.
- http://www.nrel.gov/ncpv/images/efficiency_chart.jpg
- R. E. Wasylishen, O. Knop, and J. B. Macdonald, *Solid State Commun.*, 1985, **56**, 581.
- O. Knop, R. E. Wasylishen, M. A. White, T. S. Cameron, and M. J. M. V. Oort, *Can. J. Chem.*, 1990, **68**, 412
- A. Poglitsch and D. Weber, *J. Chem. Phys.*, 1987, **87**, 6373.
- N. Onoda-Yamamuro, T. Matsuo and H. Suga, *J. Phys. Chem. Solids*, 1992, **53**, 935.
- N. Onoda-Yamamuro, T. Matsuo and H. Suga, *J. Phys. Chem. Solids*, 1990, **51**, 1383.
- N. Kitazawa, Y. Watanabe and Y. Nakamura, *J. Mat. Sci.*, 2002, **37**, 3585.
- K. Tanaka, T. Takahashi, T. Ban, T. Kondo and K. Uchida and N. Miura, *Solid State Commun.*, 2003, **127**, 619.
- I. P. Swainson, R. P. Hammond, C. Souliere, O. Knop, and W. Massa, *J. Solid State Chem.* 2003, **176**, 97.
- I. P. Swainson, M. G. Tucker, D. J. Wilson, B. Winkler, and V. Milman, *Chem. Mater.*, 2007, **19**, 2401.
- J. H. Heo, D. H. Song and S. H. Im, *Adv. Mater.*, 2014, **26**, 8179.
- A. Dymshits, A. Rotem and L. Etgar, *J. Mater. Chem. A*, 2014, **2**, 20776.
- R. Sheng, A. Ho-Baillie, S. Huang, S. Chen, X. Wen, X. Hao, and M. A. Green, *J. Phys. Chem. C*, 2015, **119**, 3545.
- N. Kedem, T. M. Brenner, M. Kulbak, N. Schaefer, S. Levchenko I. Levine, D. Abou-Ras, G. Hodes and D. Cahen, *J. Phys. Chem. Lett.*, 2015, **6**, 2469.
- R. Sheng, A. W. Y. Ho-Baillie, S. Huang, M. Keevers, X. Hao, L. Jiang, Y.-B. Cheng and M. A. Green, *J. Phys. Chem. Lett.*, 2015, **6**, 3931.
- J. H. Noh, S. H. Im, J. H. Heo, T. N. Mandal and S. I. Seok, *Nano Lett.*, 2013, **13**, 1764.
- N. J. Jeon, J. H. Noh, Y. C. Kim, W. S. Yang, S. Ryu and S. I. Seok, *Nat. Mater.*, 2014, **13**, 897.
- N. J. Jeon, J. H. Noh, Y. C. Kim, W. S. Yang, S. Ryu and S. I. Seok, *Nature*, 2015, **517**, 476.
- W. S. Yang, J. H. Noh, N. J. Jeon, Y. C. Kim, S. Ryu, J. Seo, and S. I. Seok, *Science*, 2015, **348**, 1234.
- Z.-K. Tan, R. S. Moghaddam, M. L. Lai, P. Docampo, R. Higler, F. Deschler, M. Price, A. Sadhanala, L. M. Pazos, D. Credgington, F. Hanusch, T. Bein, H. J. Snaith, and R. H Friend, *Nat. Nanotech.*, 2014, **9**, 687.
- Y. Fang, Q. Dong, Y. Shao, Y. Yuan and J. Huang, *Nat. Photonics*, 2015, **9**, 679-686.
- G. Walters, B. R. Sutherland, S. Hoogland, D. Shi, R. Comin, D. P. Sellan, O. M. Bakr and E. H. Sargent, *ACS Nano*, 2015, **9**, 9340.
- D. Priante, I. Dursun, M. S. Alias, D. Shi, V. A. Melnikov, T. K. Ng, O. F. Mohammed, O. M. Bakr, and B. S. Ooi, *Appl. Phys. Lett.*, 2015, **106**, 081902.
- Z. Gu, K. Wang, W. Sun, J. Li, S. Liu, Q. Song and S. Xiao, *Adv. Opt. Mater.*, 2016, **4**, 472-479.
- P. Tyagi, S. M. Arveson and W. A. Tisdale, *J. Phys. Chem. Lett.*, 2015, **6**, 1911.
- J. A. Sichert, Y. Tong, N. Mutz, M. Vollmer, S. Fischer, K. Z. Milowska, R. Garcia Cortadella, B. Nickel, C. Cardenas-Daw, J. K. Stolarczyk, A. S. Urban and J. Feldmann, *Nano Lett.*, 2015, **15**, 6521.
- B. Luo, Y.-C. Pu, Yi Yang, S. A. Lindley, G. Abdelmageed, H. Ashry, Y. Li, X. Li, and J. Z. Zhang *J. Phys. Chem. C*, 2015, **119**, 26772.
- D. M. Jang, K. Park, D. H. Kim, J. Park, F. Shojaei, H. S. Kang, J.-P. Ahn, J. W. Lee and J. K. Song, *Nano Lett.*, 2015, **15**, 5191.
- S. Pathak, N. Sakai, F. Wisnivesky R. Rivarola, S. D. Stranks, J. Liu, G. E. Eperon, C. Ducati, K. Wojciechowski, J. T. Griffiths, A. A. Haghighirad, A. Pellaroque, R. H. Friend and H. J. Snaith, *Chem. Mater.*, 2015, **27**, 8066.
- L. Gil-Escrig, A. Miquel-Sempere, M. Sessolo and H. J. Bolink, *J. Phys. Chem. Lett.*, 2015, **6**, 3743.
- Y. Ling, Z. Yuan, Y. Tian, X. Wang, J. C. Wang, Y. Xin, K. Hanson, B. Ma and H. Gao, *Adv. Mater.*, 2016, **28**, 305.
- Z. Yuan, Y. Shu, Y. Xin and B. Ma, *Chem. Commun.*, 2016, **52**, 3887.
- M. I. Saidaminov, A. L. Abdelhady, B. Murali, E. Alarousu, V. M. Burlakov, W. Peng, I. Dursun, L. Wang, Y. He, G. Maculan, A. Goriely, T. Wu, O. F. Mohammed and O. M. Bakr, *Nat. Commun.*, 2015, **6**, 7586.
- P. Zhao, J. Xu, X. Dong, L. Wang, W. Ren, L. Bian and A. Chang *J. Phys. Chem. Lett.*, 2015, **6**, 2622.
- Y. Yang, Y. Yan, M. Yang, S. Choi, K. Zhu, J. M. Luther and M. C. Beard, *Nat. Commun.*, 2015, **6**, 7961.
- X. Wen, A. Ho-Baillie, S. Huang, R. Sheng, S. Chen, H. Ko, and M. A. Green, *Nano Lett.*, 2015, **15**, 4644.
- C. Qiu and J. K. Grey, *J. Phys. Chem. Lett.*, 2015, **6**, 4560.

- 47 Y. Yang, M. Yang, Z. Li, R. Crisp, K. Zhu and M. C. Beard, *J. Phys. Chem. Lett.*, 2015, **6**, 4688.
- 48 T. Tachikawa, I. Karimata and Y. Kobori, *J. Phys. Chem. Lett.*, 2015, **6**, 3195.
- 49 X. Deng, X. Wen, S. Huang, R. Sheng, T. Harada, T. W. Kee, M. Green and A. Ho-Baillie *J. Phys. Chem. C*, 2016, **120**, 2542.
- 50 I. P. Swainson, C. Stock, S. F. Parker, L. Van Eijck, M. Russina and J. W. Taylor, *Phys. Rev. B*, 2015, **92**, 100303(R).
- 51 T. Baikie, N. S. Barrow, Y. Fang, P. J. Keenan, P. R. Slater, R. O. Piltz, M. Gutmann, S. G. Mhaisalkar and T. J. White, *J. Mater. Chem. A*, 2015, **3**, 9298.
- 52 F. Brivio, A. B. Walker and A. Walsh, *APL Mater.*, 2013, **1**, 042111.
- 53 J. Even, L. Pedesseau and C. Katan, *J. Phys. Chem. C*, 2014, **118**, 11566.
- 54 A. Pisoni, J. Jaćimović, O. S. Barišić, M. Spina, R. Gaál, L. Forró and E. Horváth, *J. Phys. Chem. Lett.*, 2014, **5**, 2488.
- 55 E. Mosconi, C. Quarti, T. Ivanovska, G. Ruani and F. De Angelis, *Phys. Chem. Chem. Phys.*, 2014, **16**, 16137.
- 56 R. Lindblad, D. Bi, B.-W. Park, J. Oscarsson, M. Gorgoi, H. Siegbahn, M. Odelius, E. M. J. Johansson, and H. Rensmo, *J. Phys. Chem. Lett.*, 2014, **5**, 648.
- 57 M. A. Carignano, A. Kachmar and J. Hutter, *J. Phys. Chem. C*, 2015, **119**, 8991.
- 58 J. Even, *J. Phys. Chem. Lett.*, 2015, **6**, 2238.
- 59 X. Qian, X. Gu and R. Yang, *Appl. Phys. Lett.*, 2016, **108**, 063902.
- 60 J. Even, M. Carignano and C. Katan, *Nanoscale*, 2016, **8**, 6222.
- 61 D. H. Fabini, T. Hogan, H. A. Evans, C. C. Stoumpos, M. G. Kanatzidis, and R. Seshadri, *J. Phys. Chem. Lett.*, 2016, **7**, 376.
- 62 R. P. Chapman, C. M. Widdifield, and D. L. Bryce, *Prog. Nucl. Magn. Reson. Spectrosc.*, 2009, **55**, 215.
- 63 R. E. Taylor, P. A. Beckmann, S. Bai and C. Dybowski, *J. Phys. Chem. C*, 2014, **118**, 9143.
- 64 V. G. Krishnan, S.-Q. Dou and A. Weiss, *Z. Naturforsch.*, 1991, **46a**, 1063.
- 65 M. I. Dar, M. Abdi-Jalebi, N. Arora, T. Moehl, M. Grätzel, and M. K. Nazeeruddin, *Adv. Mater.*, 2015, **27**, 7221.
- 66 S. Sharma, N. Weiden and A. Weiss, *Z. Naturforsch.*, 1987, **42a**, 1313.
- 67 O. Dmitrenko, S. Bai, P. A. Beckmann, S. van Brammer, A. J. Vega and C. Dybowski, *J. Phys. Chem. A*, 2008, **112**, 3046.
- 68 D. H. Zhou, H. Donghua, G. L. Hoatson, R. L. Vold and F. Fayon, *Phys. Rev. B*, 2004, **69**, 134104.
- 69 J. Herzfeld and A. E. Berger, *J. Chem. Phys.*, 1980, **73**, 6021.
- 70 E. Dib, T. Mineva and B. Alonso, *Annu. Rep. NMR Spectrosc.*, 2016, **87**, 175.
- 71 E. Dib, T. Mineva, P. Gaveau and B. Alonso, *Eur. Phys. J. Special Topics*, 2015, **224**, 1769.
- 72 H. Le Lann, C. Odin, B. Toudic, J. C. Ameline, J. Gallier, F. Guillaume and T. Breczewski, *Phys. Rev. B*, 2000, **62**, 5442.
- 73 C. Odin, *Annu. Rep. NMR Spectrosc.*, 2006, **59**, 117.
- 74 M. Cutajar, S. E. Ashbrook and S. Wimperis, *Chem. Phys. Lett.*, 2006, **423**, 276.
- 75 T. Bräuniger, R. Poupko, Z. Luz, H. Zimmermann and U. Haeblerlen, *J. Chem. Phys.*, 2001 **115**, 8049.
- 76 D. Massiot, F. Fayon, M. Capron, I. King, S. Le Calvé, B. Alonso, J. O. Durand, B. Bujoli, Z. Gan, and G. Hoatson, *Magn. Reson. Chem.*, 2002, **40**, 70.
- 77 A. M. A. Leguy, J. M. Frost, A. P. McMahon, V. G. Sakai, W. Kockelmann, C. H. Law, X. Li, F. Foglia, A. Walsh, B. C. O'Regan, J. Nelson, J. T. Cabral and P. R. F. Barnes, *Nat. Commun.*, 2015, **6**, 7124.
- 78 T. Chen, B. J. Foley, B. Ipek, M. Tyagi, J. R. D. Copley, C. M. Brown, J. J. Choi and S. Lee, *Phys. Chem. Chem. Phys.*, 2015, **14**, 31278.
- 79 D. Massiot, I. Farnan, N. Gautier, D. Trumeau, A. Trokiner, and J.-P. Coutures *Solid State Nucl. Magn. Reson.*, 1995, **4**, 241.
- 80 S. J. Clark, M. D. Segall, C. J. Pickard, P. J. Hasnip, M. J. Probert, K. Refson and M. C. Payne, *Z. Kristallogr.*, 2005, **220**, 567.
- 81 M. D. Segall, P. J. D. Lindan, M. J. Probert, C. J. Pickard, P. J. Hasnip, S. J. Clark and M. C. Payne, *J. Phys.: Condens. Matter*, 2002, **14**, 2717.
- 82 J. P. Perdew, K. Burke and M. Ernzerhof, *Phys. Rev. Lett.*, 1996, **77**, 3865.
- 83 H. M. Petrilli, P. E. Blöchl, P. Blaha and K. Schwarz, *Phys. Rev. B*, 1998, **57**, 14690-14697.
- 84 P. E. Blöchl, *Phys. Rev. B*, 1994, **50**, 17953.
- 85 H. J. Monkhorst and J. D. Pack, *Phys. Rev. B*, 1976, **13**, 5188.
- 86 D. D. Koelling and B. N. Harmon, *J. Phys. C: Solid State Phys.*, 1977, **10**, 3107.
- 87 S. G. Louie, S. Froyen and M. L. Cohen, *Phys. Rev. B*, 1982, **26**, 1738.
- 88 J. Cuny, S. Messaoudi, V. Alonzo, E. Furet, J.-F. Halet, E. Le Fur, S. E. Ashbrook, C. J. Pickard, R. Gautier, and L. Le Pollès, *J. Comput. Chem.*, 2008, **29**, 2279.